A numerical and stochastic approach for modeling cell population dynamics in colonic crypts undergoing asymmetric cell divisions

Sayoni Chakraborty, The University of Texas at Dallas
Nicholas Brown, Pennsylvania State University
Kayode Oluwasegun, Drexel University
Ruida Huang, University of Michigan / Baruch College
Manraj Singh Ghumman, University of Pittsburgh
Madushi Wickramasinghe, Morgan State University
Hemaho Beaugard Taboe, University of Florida
Huy Pham, Mississippi State University
Debabrata Auddya, University of Wisconsin-Madison / University of Delaware

1 Abstract

The colonic crypt has been analysed using a PDE based mathematical model to investigate the interactions between stem cells having the ability to undergo cell division. The cells are classified into three different types characterised by their ability to divide, proliferate or differentiate in a symmetric or asymmetric way. These cells are modeled as concentrations which are spatio-temporally dependent and serve as primary variables of the coupled set of PDEs. The set of equations are analytically and numerically solved using the method of characteristics and by using a stochastic approach. While previous models have considered a simplistic kinetic set of equations for the cell types, the present model increases the modeling fidelity by including additional variables which closely mimic the biological processes. The results indicate a close agreement of the analytical solutions with numerical simulations along with a detailed demonstration of stochastic methods which overall highlight a robust numerical framework for modeling cell population dynamics in colonic crypts.

2 Introduction

The single layer of epithelial cells lining the colon is investigated in order to understand cell division, proliferation and differentiation using mathematical modeling. These stem cells are thought to reside at the bottom of the colonic crypt which assist in the production and regeneration of cells which eventually move up and are removed by shedding into the lumen of the colon. In order to maintain physiological homeostasis, there is a balance between the number of cells which are removed due to cell differentiation or cell death with new cell addition. A shift in this balance causes changes in critical concentrations of cells responsible for cancer progression. The colonic crypts has been studied using a one dimensional model which captures the dynamics of cell division, proliferation and differentiation known to trigger an array of pathological abnormalities such as colorectal cancer [1].

The onset of these pathological disorders often initiate with visible markers highlighting the increased presence of proliferated or differentiated cells which eventually lead to progressive cancerous conditions [2]. The challenges in predicting the spatio-temporal dynamics of pathological transformation in colonic crypts due to abnormal stem cell divisions serve as a fundamental motivation to formulate numerical methods [3, 4]. Some of the popular mathematical models which has been utilised to address cell density populations in colonic crypts use the ordinary differential equations (ODE) for capturing evolutionary cell dynamics. The idea is to idealise the distribution of cell types as concentrations and numerically predict their temporal behaviour. In this study we use a partial differential equation (PDE) formulation to model

proliferation and differentiation using three different cell types. These species are coupled to each other using kinetic equations having rate coefficients which determine their production or depletion.

Tomlinson and Bodmer's seminal model considered the dynamics of cell division, differentiation, and apoptosis within the colonic crypt, demonstrating how variations in these processes can precipitate exponential growth of stem cell populations [5]. Similar mathematical models were proposed by [6, 7, 8, 9] with more recent contributions using statistical modeling and machine learning methods [10, 11, 12]. In this study a one dimensional model has been chosen as the numerical domain and we consider three different types of cells, C, indicating healthy cells capable of progressive division, P, indicating proliferating cells which undergo regressive division and D, indicating differentiated cells which no longer undergo division. In the following sections the PDE model is formulated and analytical methods derived which is further used to numerically[1] solve the problem. Later, a stochastic model is developed and results are shown which further illustrate cell population dynamics. Additionally, detailed derivations used in the modeling process to obtain analytical and numerical solutions are included in the appendix for interested readers.

3 Methods

3.1 PDE Model

As mentioned above, in a colonic crypt there are three main cell types representing dividing cells, proliferative (non-cycling) cells and differentiated cells(unable to divide). Our model utilises all three types namely stem cells (C), proliferative cells (P), and differentiated cells (D). We are considering asymmetric division of stem cells and proliferative cells as well. The following kinetic scheme is considered.

$$C \xrightarrow{k_1} C + P$$
$$P \xrightarrow{k_2} P + D$$

where k_1 is the rate at which C cell divides (asymmetrically) into C+P and k_2 is the rate at which P cell divides(asymmetrically) into P+D.

- **Assumptions:**
  1. The crypt is one dimensional with height L (Figure 2).
  2. All the cells have the same size and are rigid. That is, the total density of cells per unit length is expressed as $C + P + D = \rho_{max}$, for some constant ρ_{max}
  3. Upon division, the creation of a new cell will push the above cells
  4. There is no cell death within the crypt and the only way for cells to exit from the crypt is to be pushed out at the top
  5. The cell distribution is uniform.

Using the two equations above, the following are the rate of growth of each type of cell:

[1]Some sections of the code were generated using AI assisted technology such as ChatGPT

$$\frac{dC}{dt} = 0 \tag{1}$$

$$\frac{dP}{dt} = k_1 C \tag{2}$$

$$\frac{dD}{dt} = k_2 P \tag{3}$$

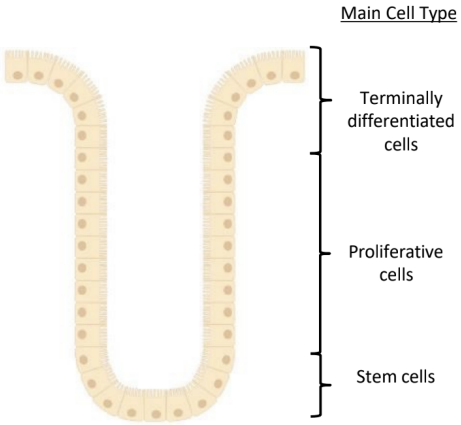

Figure 1

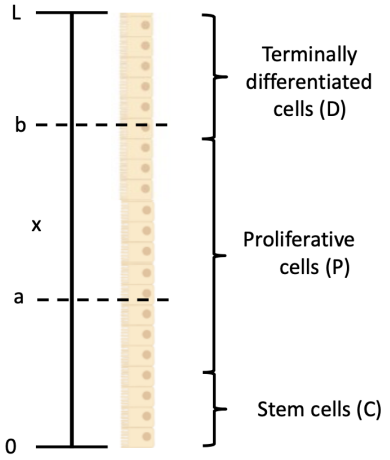

Figure 2

We are using a continous model with respect to time and space. $C(x,t), P(x,t)$, and $D(x,t)$ are the density of stem cells, proliferative cells, and differentiated cells respectively at position x and time t. The construction of an appropriate spatial model initiates with an arbitrary interval $[a,b]$ (Figure 2). In order to develop the PDE model, we need the rates of change of stem cells, proliferative cells, and differentiated cells. According to the conservation law, rate of change of cells = Flux in - Flux Out + The cell production in $[a,b]$. Flux of the cells into the interval [a,b] = Total production of the cells in [a,b] times the proportion of that respective cells at position $x = a$. Similarly, flux out of the cells will be = total production of cells in [a,b] times the proportion of that respective cells at position $x = a$. Total production of proliferative cells on [a,b] is $\int_a^b k_1 C dx$. Similarly, the total production of differentiated cells on [a,b] = $\int_a^b k_2 P dx$

Hence the expressions for partial derivatives for rate of change of each cells are as follows:

$$\frac{\partial}{\partial t}\int_a^b C dx = \int_0^a (k_1 C + k_2 P) dx \left(\frac{C}{\rho_{max}}\right)\Big|_{x=a} - \int_0^b (k_1 C + k_2 P) dx \left(\frac{C}{\rho_{max}}\right)\Big|_{x=b} \tag{4}$$

$$\frac{\partial}{\partial t}\int_a^b P dx = \int_0^a (k_1 C + k_2 P) dx \left(\frac{P}{\rho_{max}}\right)\Big|_{x=a} - \int_0^b (k_1 C + k_2 P) dx \left(\frac{P}{\rho_{max}}\right)\Big|_{x=b} + \int_a^b k_1 C dx \tag{5}$$

$$\frac{\partial}{\partial t}\int_a^b D dx = \int_0^a (k_1 C + k_2 P) dx \left(\frac{D}{\rho_{max}}\right)\Big|_{x=a} - \int_0^b (k_1 C + k_2 P) dx \left(\frac{D}{\rho_{max}}\right)\Big|_{x=b} + \int_a^b k_2 P dx \tag{6}$$

For arbitrary $[a,b]$, we have the following system of PDEs through rearranging (Appendix 6.1)

$$\frac{\partial C}{\partial t} + \frac{\partial}{\partial x}\left(\int_0^x (k_1 C(z,t) + k_2 P(z,t)) dz \frac{C(x,t)}{\rho_{max}}\right) = 0 \tag{7}$$

$$\frac{\partial P}{\partial t} + \frac{\partial}{\partial x}\Big(\int_0^x (k_1 C(z,t) + k_2 P(z,t))dz \frac{P(x,t)}{\rho_{max}} \Big) = k_1 C \tag{8}$$

$$\frac{\partial D}{\partial t} + \frac{\partial}{\partial x}\Big(\int_0^x (k_1 C(z,t) + k_2 P(z,t))dz \frac{D(x,t)}{\rho_{max}} \Big) = k_2 P \tag{9}$$

Equation (8),(9),(10) represents a model which are non-local PDEs. So, introducing new variables to convert non-local PDEs to local PDEs:

$$S = \int_0^x C(z,t)dz$$
$$R = \int_0^x P(z,t)dz$$
$$T = \int_0^x D(z,t)dz$$

Now, we have the following local PDEs :

$$\begin{aligned} \tfrac{\partial S}{\partial t} + \Big(\tfrac{k_1}{\rho_{max}} S + \tfrac{k_2}{\rho_{max}} R \Big) \tfrac{\partial S}{\partial x} &= 0 \\ \tfrac{\partial R}{\partial t} + \Big(\tfrac{k_1}{\rho_{max}} S + \tfrac{k_2}{\rho_{max}} R \Big) \tfrac{\partial R}{\partial x} &= k_1 S \\ \tfrac{\partial T}{\partial t} + \Big(\tfrac{k_1}{\rho_{max}} S + \tfrac{k_2}{\rho_{max}} R \Big) \tfrac{\partial T}{\partial x} &= k_2 R \end{aligned} \tag{10}$$

This PDEs have similar forms to the inviscid Burger's equation, we can solve this system analytically when given an initial condition for S, R and T by applying method of characteristics. The above PDE models can be converted to the following system of ODEs.

$$\begin{aligned} \frac{dS}{ds} &= 0 \\ \frac{dR}{ds} &= k_1 S \\ \frac{dT}{ds} &= k_2 R \\ \frac{dx}{ds} &= \frac{k_1}{\rho_{max}} S + \frac{k_2}{\rho_{max}} R \\ \frac{dt}{ds} &= 1 \end{aligned} \tag{11}$$

3.1.1 Numerical Solution

We can now simplify the system of ODEs and get a numerical solution. We will use the following equation for our numerical simulation.

$$S = S(x_0, 0)$$
$$t = s$$
$$R^{new} = R^{old} + \frac{1}{10} k_1 \rho_{max} x_0 dt$$
$$T^{new} = T^{old} + \frac{1}{10} \rho_{max} (k_1 S + 4) k_2 x_0 dt$$

$$x^{new} = \frac{1}{10}\left(\frac{1}{2}k_1k_2t^2 + (4k_2 + k_1)t\right)x_0 + x_0$$

We implemented the numerical solution using MATLAB and compare with the analytic solution and calculated the error. The numerical solution confirms the predicted behaviour of the system.

3.2 Probabilistic Model

In this section, we focus on simulating the spatial distribution of crypt cells in various stages of colonic cancer (healthy, FAP, adenoma) to gain insights into how cell division patterns affect the development of the disease. This could significantly aid in the early detection and assessment of colonic cancer and provide insights into its early development mechanisms.

Our primary goal is to simulate and analyze the crypt cells' spatial distribution under various health conditions to understand how different division rates and division types (symmetric vs. asymmetric) influence colonic cancer's progression. This model aims to serve as a predictive tool for disease stages and explore potential interventions.

3.2.1 Naive Branching Process Model

We begin with a naive approach based on branching processes to describe the cell division within the crypts. The process is characterized as follows:

$$C \to \begin{cases} C + C, & \text{rate } k_1, \text{ probability } p, \text{ (symmetric division)} \\ C + P, & \text{rate } k_1, \text{ probability } 1 - p, \text{ (asymmetric division)} \end{cases}$$

$$P \to \begin{cases} P + P, & \text{rate } k_2, \text{ probability } q, \text{ (symmetric division)} \\ P + D, & \text{rate } k_2, \text{ probability } 1 - q, \text{ (asymmetric division)} \end{cases}$$

where C, P, and D represent stem, proliferative, and differentiated cells, respectively. This model is based on Poisson processes, reflecting the inherent randomness of cellular division when population pressures are low. While the branching process model provides a foundational understanding, it exhibits significant limitations:

- **Directionality of Division:** The model does not account for the spatial dynamics where stem cells at the base of the crypt push newly formed cells upward. This upward movement is crucial for maintaining the structural integrity and functional zoning within the crypt.
- **Bounded System:** In reality, the crypt maintains a relatively stable size, implying a bounded system in terms of cell numbers. The naive model allows for unbounded growth, which is biologically unrealistic.

One possible solution to these limitations is the Continuous-time Markovian Model, which incorporates spatial constraints and directed movements to more accurately mirror the crypt dynamics. We will also adjust the system boundaries to reflect the stable crypt size.

3.2.2 Continous Time Markov Chain Model (CTMC)

Let $\Omega = \{C, P, D\}^N$ be the state space representing all possible configurations of N cells in a 1-D array, where each cell is in one of three states: stem cell (C), proliferative cell (P), or differentiated cell (D).

Define the stochastic process $\{X(t), t \geq 0\}$ on Ω, where $X(t) = (X_1(t), \ldots, X_N(t))$ and $X_i(t) \in$

$\{C, P, D\}$ represents the state of the i-th cell at time t. The infinitesimal generator matrix $Q = (q_{x,y})_{x,y\in\Omega}$ of this CTMC is defined as follows:

For $x = (x_1, \ldots, x_N)$ and $y = (y_1, \ldots, y_N)$ in Ω, and $i \in \{1, \ldots, N-1\}$:

Stem cell division at position i:

$$q_{x,y} = \begin{cases} p \cdot k_1, & \text{if } x_i = C, y_i = C, y_{i+1} = C, \text{ and } y_j = x_{j-1} \text{ for } j > i+1, \\ (1-p) \cdot k_1, & \text{if } x_i = C, y_i = C, y_{i+1} = P, \text{ and } y_j = x_{j-1} \text{ for } j > i+1, \\ 0, & \text{otherwise.} \end{cases}$$

Proliferative cell division at position i:

$$q_{x,y} = \begin{cases} q \cdot k_2, & \text{if } x_i = P, y_i = P, y_{i+1} = P, \text{ and } y_j = x_{j-1} \text{ for } j > i+1, \\ (1-q) \cdot k_2, & \text{if } x_i = P, y_i = P, y_{i+1} = D, \text{ and } y_j = x_{j-1} \text{ for } j > i+1, \\ 0, & \text{otherwise.} \end{cases}$$

Diagonal elements:

$$q_{x,x} = -\sum_{y \neq x} q_{x,y} \text{ (Completeness of Probability)}$$

This model captures the "pushing out" effect near the top of the crypt through the condition $y_j = x_{j-1}$ for $j > i+1$ in the transition rates. This ensures that when a cell divides, all cells above it are pushed upwards, and the cell at position N is implicitly removed from the system.

However, there is a major pitfall when we apply this model to simulate the spatial structure of crypts of different health states. To illustrate this idea, we need the following Theorem:

Theorem 3.1. *Let $\theta_C(t)$, $\theta_P(t)$, and $\theta_D(t)$ be the expected densities of stem cells, proliferative cells, and differentiated cells, respectively, at time t. As $N \to \infty$ and $t \to \infty$:*

(a) If $k_1 < k_2$ and $p < 1$, then $\theta_C(t) \to 0$.

(b) If $k_1 \geq k_2$, then $\theta_C(t) \to 0$ if and only if $\frac{p}{q} = \frac{k_2}{k_1}$ and $pk_1 < k_2$.

The theorem provides crucial insights into the asymptotic behavior of cell populations in colonic crypts. Experimental observations of colonic crypts reveal distinct spatial distributions of cell types in different health states:

- **Healthy Crypts:** Stem cells (C) are confined to the base, proliferative cells (P) occupy the lower portion, and differentiated cells (D) dominate the upper regions. Notably, $\theta_P \to 0$ as we approach the top of the crypt.
- **Familial Adenomatous Polyposis (FAP):** Similar to healthy crypts, but with an expanded proliferative zone. Still, $\theta_P \to 0$ at the crypt top.
- **Adenoma:** Disrupted structure with proliferative cells persisting to the top ($\theta_P \not\to 0$). Stem cells may be found in upper crypt regions.

Our theorem provides the following insights:

1. When $k_1 < k_2$ (biologically common), $\theta_C \to 0$ as $t \to \infty$, provided $p < 1$.
2. When $k_1 \geq k_2$, $\theta_C \to 0$ if and only if $\frac{p}{q} = \frac{k_2}{k_1}$ and $pk_1 < k_2$.

These results highlight several limitations of our current model:

- **Stem Cell Extinction:** In the common case where $k_1 < k_2$, our model predicts stem cell extinction ($\theta_C \to 0$). This fails to capture the persistent stem cell population observed in healthy and FAP crypts.
- **Proliferative Cell Equilibrium:** When $k_1 < k_2$, our model suggests that proliferative cells reach a non-zero equilibrium ($\theta_P = \frac{pk_1}{k_2}$). This contradicts the observation that $\theta_P \to 0$ at the crypt top in healthy and FAP states.

To better understand the model's implications, we introduce a definition of cellular equilibrium:

Definition 3.1 (Cellular Equilibrium)**.** *For a cell type $r \in \{C, P, D\}$, given a state space and parameter set $\Theta = (N, k_1, k_2, p, q)$, we say r is in equilibrium of if there exists $\tau \geq 0, M \leq N, \theta \in (0, 1)$ such that*

$$\forall S \subset [M, N], \mathbb{E}[t : |\theta_r(t) - \theta| \geq \frac{1}{N}, t > \tau] = +\infty \tag{12}$$

where τ is the first time the system reaches equilibrium, and the density is evaluated on subset $S \in [M, N]$

This definition captures the idea that a cell type is in equilibrium if its expected density never reaches zero in finite time. In our model:

- When $k_1 < k_2$, $\theta_C \to 0$ as $t \to \infty$, implying stem cells are not in equilibrium.
- Proliferative cells (P) are always in equilibrium when $k_1 < k_2$, as $\theta_P \to \frac{pk_1}{k_2} > 0$.

This presents a paradox: our model predicts proliferative cell equilibrium in all cases, failing to distinguish between healthy, FAP, and adenoma states. In reality, persistent proliferative cells throughout the crypt (including the top) are indicative of adenoma, not healthy or FAP crypts.

3.2.3 Towards a More Realistic Model

To address these limitations and better capture the observed crypt dynamics, we propose incorporating spatial dependence into our model:

- **Spatial-dependent Division Probabilities:** Define $p(x)$ and $q(x)$ as functions of crypt position x, such that:

  $$\frac{d}{dx}p(x) < 0, \quad \frac{d}{dx}q(x) < 0 \tag{13}$$

  This reflects the biological observation that cells are less likely to undergo symmetric division and more likely to differentiate as they move up the crypt. One specific model the has been shown (see section 4.2) to work well is to use the following function:

  $$p(i) = 1 - p_0 \cdot \exp(\lambda_p \cdot i/N) \tag{14}$$
  $$q(i) = 1 - q_0 \cdot \exp(\lambda_q \cdot i/N) \tag{15}$$

- **Spatially-varying Division Rates:** Consider $k_1(x)$ and $k_2(x)$ to account for position-dependent division rates, potentially incorporating signaling gradients (e.g., Wnt pathway) known to influence cell behavior along the crypt axis. One way to model these rates using a Gaussian distribution:

  $$k_1(i) = k_1 \cdot \exp\left(-\frac{(i-\mu)^2}{2\sigma^2}\right)$$

$$k_2(i) = k_2 \cdot \exp\left(-\frac{(i-\mu)^2}{2\sigma^2}\right)$$

where $\mu = \frac{N}{3}$ and σ has been chosen to be large to ensure a wide spread.

By incorporating these spatial dependencies, we aim to develop a model that can:

(i) Maintain a stable stem cell population at the crypt base.

(ii) Produce a proliferative zone that diminishes towards the crypt top in healthy and FAP states.

(iii) Allow for the possibility of expanded proliferative zones and mislocalized stem cells in adenoma states.

4 Results

4.1 Deterministic Model

4.1.1 Analytic Solution

Since our method allows us to create the local PDE model which can be solved given an initial condition analytically for a particular example, we consider that the initial distribution of stem cells is uniform and covers 10 percent of he total number of cells, and proliferative cells covers 40 percent of the total and differentiated cells covers 50 percent of the total number of cells along the crypt. Then we have the following initial conditions for S, R and T.

$$\begin{aligned} S(x,0) &= \tfrac{\rho_{max}}{10}x \\ R(x,0) &= \tfrac{4\rho_{max}}{10}x \\ T(x,0) &= \tfrac{5\rho_{max}}{10}x \end{aligned} \tag{16}$$

Using the method of characteristics, we get the exact solution as follows.

$$\begin{aligned} S(x,t) &= \rho_{max}\tfrac{x}{(10+(4k_2+k_1)t+\frac{1}{2}k_1k_2t^2)} \\ R(x,t) &= \rho_{max}\tfrac{(k_1t+4)x}{(10+(4k_2+k_1)t+\frac{1}{2}k_1k_2t^2)} \\ T(x,t) &= \rho_{max}\tfrac{(\frac{1}{2}k_1k_2t^2+4k_2t+5)x}{(10+(4k_2+k_1)t+\frac{1}{2}k_1k_2t^2)} \end{aligned} \tag{17}$$

$S(x,t), R(x,t)$, and $T(x,t)$ represents the cumulative stem cell distribution and proliferative cell distribution and terminative differentiated cell distribution respectively. So we can get the actual cell distribution $C(x,t), P(x,t)$, and $D(x,t)$ by computing the derivative of the above solution with respect to x. According to our assumption that the cell distribution is uniform and also our simple choice of initial conditions, we got $S(x,t), R(x,t)$, and $T(x,t)$ as a function of t times x. Hence derivative of these equations with respect to x will be easily computable.

4.1.2 Numerical Solution

We also use the method of characteristics to obtain the numerical solution and compare with the true solution. We choose the parameters:

$$L = 2, \rho_{max} = 80, k_1 = 1, k_2 = 1.5,$$

and the time interval is $[0, 5]$. We discretize the problem with 200 spatial grid points and 500 time grid points The results are shown in figures 3, 4, 5:

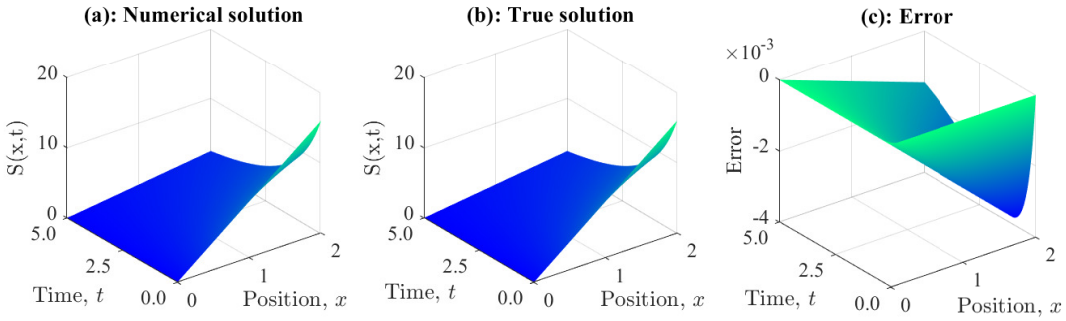

Figure 3: S component

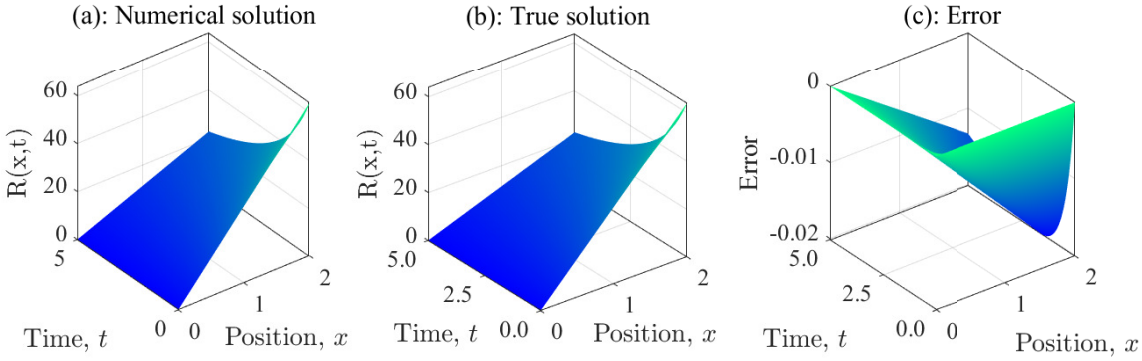

Figure 4: R component

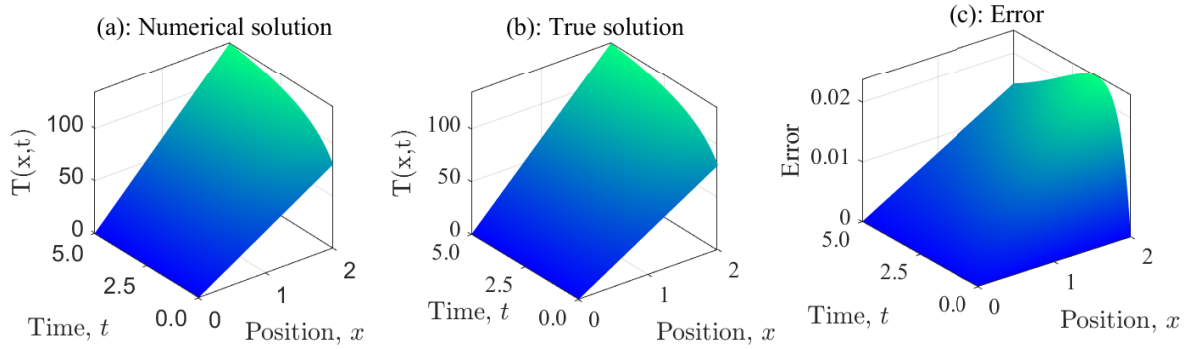

Figure 5: T component

4.2 Stochastic Modeling

4.2.1 Simple Continuous Time Markov Chain Model

We first implemented a basic Continuous Time Markov Chain (CTMC) model to investigate the spatial distribution of cells in colonic crypts.

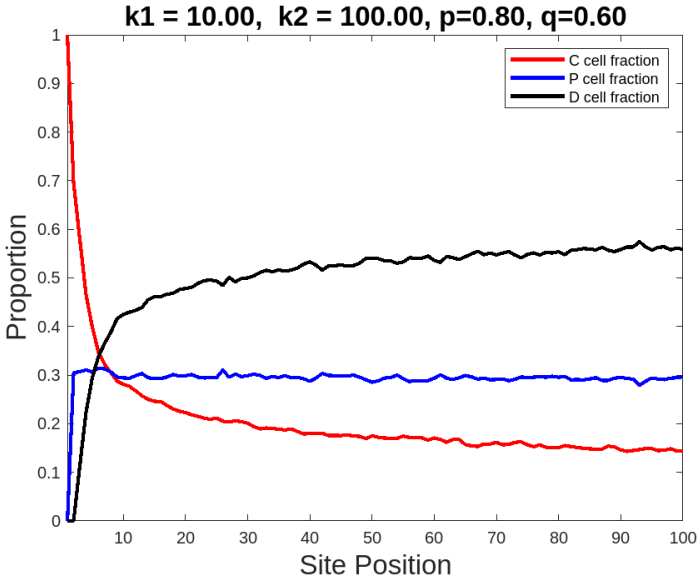

Figure 6: Snapshot of cell distribution in the simple CTMC model. C: stem cells, P: proliferative cells, D: differentiated cells.

Figure 6 shows a representative snapshot of the cell distribution. In this model, we observe:

- A relatively uniform distribution of cell types throughout the crypt.
- Presence of stem cells (C) throughout the crypt, which doesn't align with biological observations.
- No clear compartmentalization of proliferative (P) and differentiated (D) cells.

These results highlight the limitations of the simple CTMC model in capturing the spatial heterogeneity observed in real colonic crypts.

4.2.2 Properties of Simple CTMC Model

To understand the long-term behavior of the simple CTMC model, we analyzed its asymptotic behavior and equilibrium state.

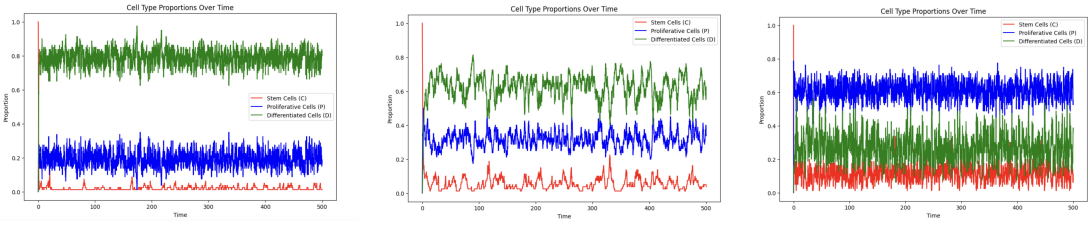

Figure 7: Temporal evolution of cell populations in the simple CTMC model. Solid lines represent 1 simulation run.

Figure 7 illustrates the temporal evolution of cell populations. We observe:

- After an initial transient period, the populations reach a stable equilibrium.
- The stem cell population (C) on the left most plot approaches zero, consistent with our theoretical predictions when $k_1 < k_2$, where as the one corresponding to $k_1 > k_2$ has fluctuating $N_C(t)$.

- Proliferative (P) and differentiated (D) cells maintain non-zero equilibrium values.

These results confirm our theoretical analysis and implies that it is necessary to capture the spatial organization observed in healthy crypts. We will present in the following sections two control methods to simulate the stochastic process that gives the desired property of spatial distribution of different cells on the crypt.

4.2.3 Model with Decreasing Symmetric Division Rate, Controlling k_1/k_2

To address the limitations of the simple model, we implemented a modified CTMC model with spatially-dependent symmetric division rates (3.2.3), while controlling the ratio k_1/k_2.

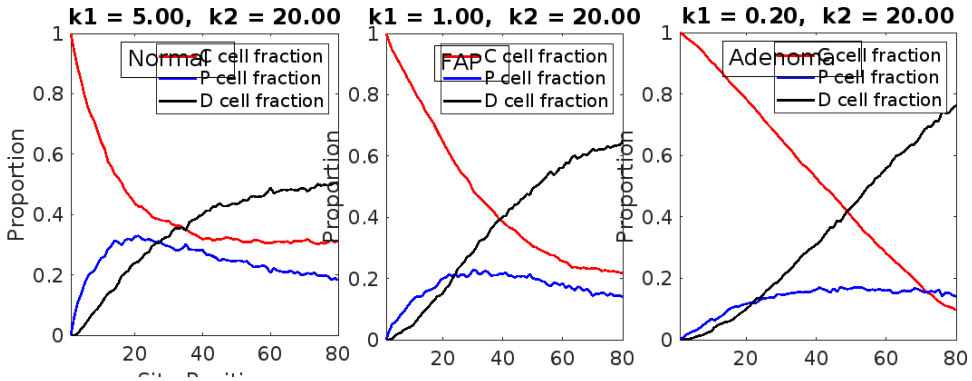

Figure 8: Spatial distribution of cell types in the modified CTMC model with decreasing symmetric division rate, controlling k_1/k_2. From left to right - Normal: $k_1/k_2 = 0.25$, FAP: $k_1/k_2 = 0.05$, Adenoma: $k_1/k_2 = 0.01$.

Figure 8 shows the spatial distribution of cell types for different ratios of $\frac{k_1}{k_2}$. We observe:

- A more realistic compartmentalization of cell types, with stem cells concentrated at the crypt base.
- The extent of the proliferative zone varies with the $\frac{k_1}{k_2}$ ratio, potentially mimicking different health states.
- A gradual transition from proliferative to differentiated cells along the crypt axis.

corresponding biological interpretation:

4.2.4 Model with Decreasing Symmetric Division Rate, Controlling λ_q

In our final model, we explored the effects of varying the exponential parameter λ_q, which governs the changing rate of proliferative cell symmetric division probability, while maintaining spatially-dependent stem cell division.

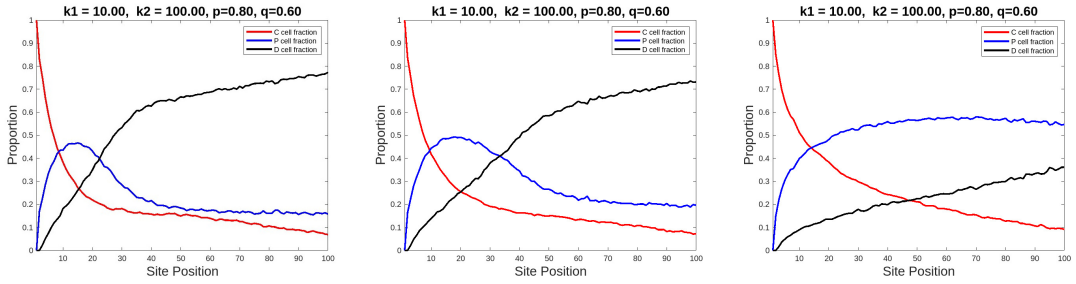

Figure 9: Spatial distribution of cell types in the modified CTMC model with decreasing symmetric division rate, controlling λ_q. Normal: $\lambda_q = 6$, FAP: $\lambda_q = 4$, Adenoma: $\lambda_q = 0.5$.

Figure 9 illustrates the impact of different λ_q values on crypt structure. Key observations include:

- Lower λ_q values lead to an expanded proliferative zone, potentially mimicking FAP or early adenoma states, whereas higher λ_q values result in a more rapid transition to differentiated cells, similar to healthy crypts.
- The stem cell compartment remains localized to the crypt base across all λ_q values.

corresponding biological interpretation:

4.3 Probabilistic Model

Using the probabilistic model, we have resulted in a density graph that is similar to Dr. Boman's hypothesis. Using an $O(n^3 + n^2)$ algorithm, we can create a density curve, as well as a time curve.

4.3.1 Patterns

Upon experimenting with the parameters in the program, a conclusion that can be made is that the state of a crypt can be determined by the ratio $\frac{p}{q}$.

4.3.2 Normal Crypt

A crypt is normal when the statement, $\frac{p}{q} \approx 1$ holds. Below is the figure compared to Dr. Boman's prediction.

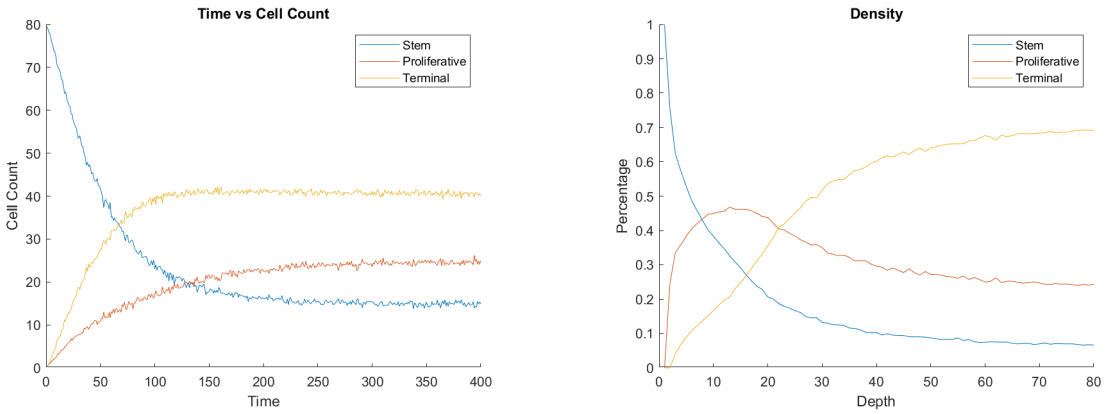

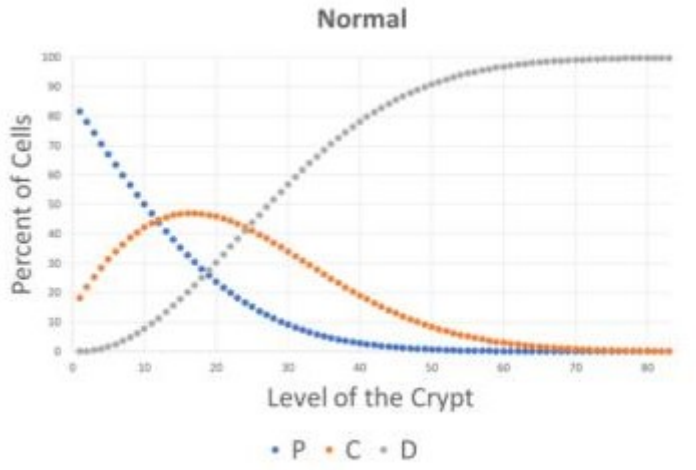

Figure 11: Normal crypt

4.3.3 FAP Crypt

A crypt is normal when the statement, $\frac{p}{q} \approx \frac{1}{3}$ holds. The figure below is a comparison to Dr. Boman's prediction.

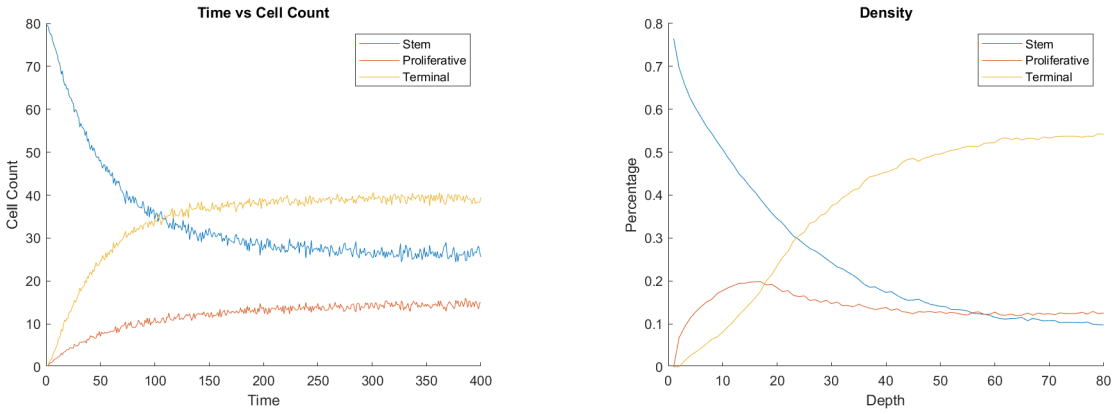

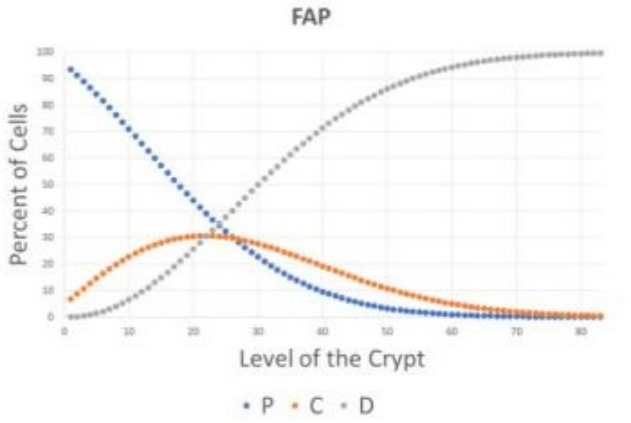

Figure 13: FAP crypt

4.3.4 Adenoma Crypt

A crypt is normal when the statement, $\frac{p}{q} \approx \frac{1}{10}$ holds. The figure below is a comparison to Dr. Boman's prediction.

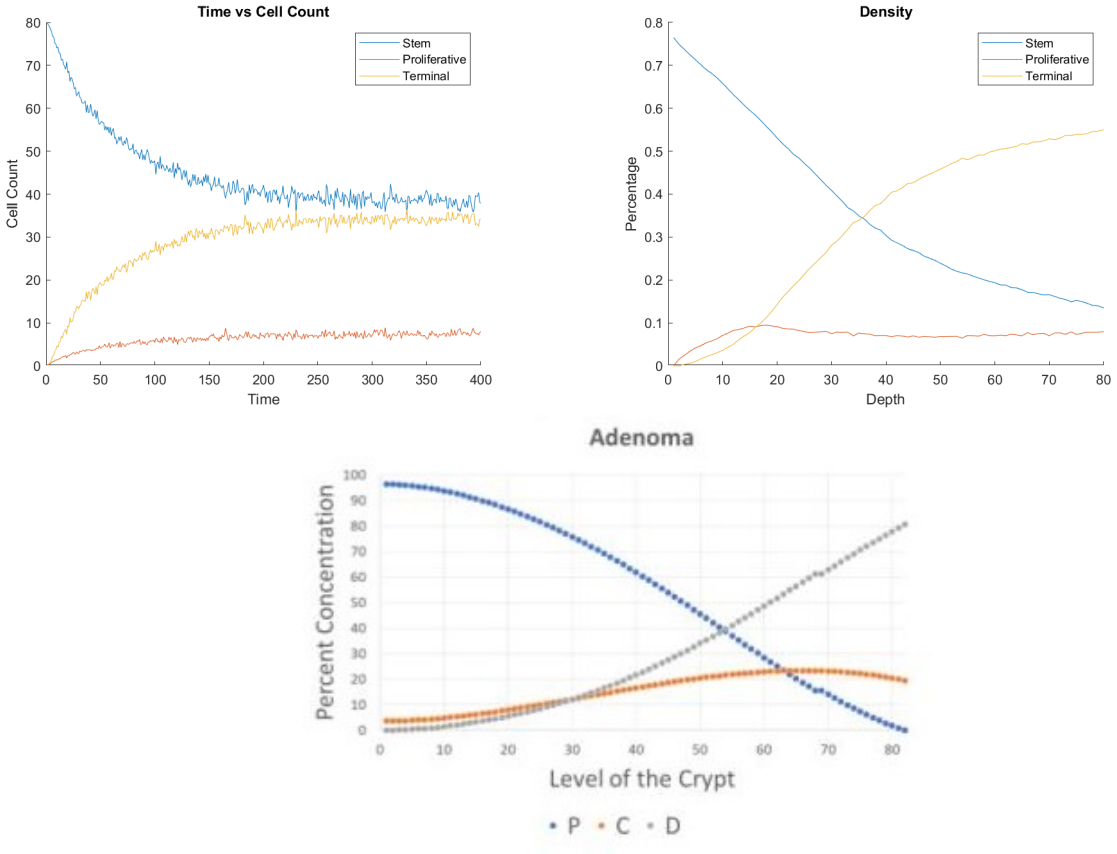

Figure 14: Adenoma crypt

5 Discussion

In this PDE representation of cell population dynamics of the colonic crypt, a novel approach of asymmetric cell division using numerical, analytical and probabilistic methods is presented. The idea develops on a previously established model of cellular kinetics in colonic crypts which considers two different species of cells, developed in a previous GSMMC workshop from 2022. The present work extends that idea into three different cell types. While time limitations prevented extensive tests of the model, we hope that it may provide insight into the transition from normal to abnormal dynamics of the cell populations in the colonic crypt. The deterministic model highlights the numerical and analytical solutions and validates by measuring the corresponding error between them.

The modularity of this work also allows it to be extended beyond this communication. The rate constants used to define the kinetics of cell production are considered constants for simplicity. However, experimental studies have highlighted the spatial dependence of the rate parameters in colonic crypts. Inclusion of this parametric property allows improvised understanding of cellular behaviour and interactions. Modulating the rate constants also entails changes in the numerical framework thereby serving as a possible direction of study in mathematical analysis. For this problem, a fixed one dimensional domain was assumed, which is a simplified approximation of the colonic crypt. Future possibilities of extending this model can include expansion of the computational domain into higher dimensions, realistic geometries of the crypt as well as

incorporating growth and remodeling.

6 Appendix

6.1 Analytical Solution

Equation 4, can be rewritten as follows.

$$\frac{\partial}{\partial t}\int_a^b C dx = -\int_a^b \frac{\partial}{\partial x}\Big(\int_0^x (k_1 C + k_2 P)\frac{C(z,t)}{\rho_{max}} dz\Big) dx$$

$$\int_a^b \Big(\frac{\partial C}{\partial t} + \frac{\partial}{\partial x}\Big[\frac{C(z,t)}{\rho_{max}}\int_0^x (k_1 C + k_2 P) dz\Big]\Big) dx = 0 \tag{18}$$

Similarly Equation 5 can be rewritten as

$$\int_a^b \Big(\frac{\partial P}{\partial t} + \frac{\partial}{\partial x}\Big[\frac{P(z,t)}{\rho_{max}}\int_0^x (k_1 C + k_2 P) dz\Big] - k_1 C\Big) dx = 0 \tag{19}$$

Similarly Equation 6 can be rewritten as

$$\int_a^b \Big(\frac{\partial D}{\partial t} + \frac{\partial}{\partial x}\Big[\frac{D(z,t)}{\rho_{max}}\int_0^x (k_1 C + k_2 P) dz\Big] - k_2 P\Big) dx = 0 \tag{20}$$

From Equation 18, 19 and 20 we can obtain

$$\frac{\partial C}{\partial t} + \frac{\partial}{\partial x}\Big(\frac{C(z,t)}{\rho_{max}}\int_0^x (k_1 C + k_2 P) dz\Big) = 0 \tag{21}$$

$$\frac{\partial P}{\partial t} + \frac{\partial}{\partial x}\Big(\frac{P(z,t)}{\rho_{max}}\int_0^x (k_1 C + k_2 P) dz\Big) = k_1 C \tag{22}$$

$$\frac{\partial D}{\partial t} + \frac{\partial}{\partial x}\Big(\frac{D(z,t)}{\rho_{max}}\int_0^x (k_1 C + k_2 P) dz\Big) = k_2 P \tag{23}$$

Now by conservation equation we have

$$C_t + f_C = 0$$

$$\frac{\partial C}{\partial t} + \frac{\partial f_C}{\partial x} = 0$$

$$\int_0^x \Big(\frac{\partial C}{\partial t} + \frac{\partial f_C}{\partial x}\Big) dx = 0$$

$$\int_0^x \frac{\partial C}{\partial t} dx + f_C = 0$$

By using Equation 21

$$\frac{\partial}{\partial t}\int_0^x C(z,t) dz + \frac{C(x)}{\rho_{max}}\int_0^x (k_1 C + k_2 P) dz = 0$$

$$\frac{\partial}{\partial t}\int_0^x C(z,t) dz + \frac{1}{\rho_{max}}\int_0^x (k_1 C + k_2 P) dz \frac{\partial}{\partial x}\int_0^x C(z,t) dz = 0$$

By letting

$$S = \int_0^x C(z,t) dz$$

$$R = \int_0^x P(z,t)dz$$

we have Equation 4

$$\frac{\partial S}{\partial t} + \Big(\frac{k_1}{\rho_{max}} S + \frac{k_2}{\rho_{max}} R\Big)\frac{\partial S}{\partial x} = 0$$

Similarly by conservation equation we have

$$P_t + f_P = k_1 C$$
$$\int_0^x \frac{\partial P}{\partial t} dx + f_P = \int_0^x k_1 C(x,t)dz$$

By using Equation 22 we have Equation 5 as follows.

$$\frac{\partial}{\partial t}\int_0^x P(z,t)dz + \frac{1}{\rho_{max}}\int_0^x (k_1 C + k_2 P)dz \frac{\partial}{\partial x}\int_0^x P(z,t)dz = \int_0^x k_1 C(z,t)dz$$
$$\frac{\partial R}{\partial t} + \Big(\frac{k_1}{\rho_{max}} S + \frac{k_2}{\rho_{max}} R\Big)\frac{\partial R}{\partial x} = k_1 S$$

Similar manner we can observe Equation 6 by using $T = \int_0^x D(z,t)dz$

$$\frac{\partial T}{\partial t} + \Big(\frac{k_1}{\rho_{max}} S + \frac{k_2}{\rho_{max}} R\Big)\frac{\partial T}{\partial x} = k_2 R$$

Now the Equation 4 leads to the following set of differential equations.

$$\frac{dS}{ds} = 0, \quad \frac{dt}{ds} = 1, \quad \frac{dx}{ds} = \frac{k_1}{\rho_{max}} S + \frac{k_2}{\rho_{max}} R \tag{24}$$

Initial conditions in Equation 16 will leads the above first differential equation in Equation 24 into

$$S = S(0) \rightarrow S = \frac{\rho_{max}}{10} x_0 \tag{25}$$

Initial conditions in Equation 16 will leads the second second differential equation in Equation 24 into

$$t = s$$

Similarly Equation 5 leads to

$$\frac{dR}{ds} = k_1 S$$

Initial conditions in Equation 16 will leads the above differential equation into

$$R = \frac{x_0 \rho_{max}}{10}(k_1 t + 4) \tag{26}$$

Similarly Equation 6 leads to

$$\frac{dT}{ds} = k_2 R$$

Initial conditions in Equation 16 will leads the above differential equation into

$$T = \frac{x_0 \rho_{max}}{10}(\frac{k_1 k_2 t^2}{2} + 4k_2 t + 5) \tag{27}$$

Solving the third differential equation in Equation 24 give the solution for x as

$$x = \frac{1}{10}\Big(\frac{k_1 k_2 t^2}{2} + (4k_2 + k_1)t\Big)x_0 + x_0$$

Solving for x_0:

$$x_0 = \frac{10x}{10 + (4k_2 + k_1)t + \frac{k_1 k_2 t^2}{2}}$$

Plugging x_0 back in Equation 25,26 and 27 gives us the solution for S, R and T as in Equation 17.

6.2 MATLAB code for the deterministic model

In this section, we provide a code for the PDE model discussed above. The parameters can be changed for different models. One honourable mention is that our code is modified from a sample provided by ChatGPT.

```
global k1 k2 rho

rho = 80;
k1 = 1;
k2 = 1.5;
x0 = 0;
xend = 2;
t0 = 0;
tend = 5;
Nx = 201;
Nt = 501;

[x,t,u,v,w] = MOC(x0,xend,t0,tend,Nx,Nt);
[X,T] = meshgrid(x,t);
[utrue,vtrue,wtrue] = truesol(X,T);

%%
figure;
surf(X, T, u');
shading interp;
xlabel('x');
ylabel('Time');
zlabel('S(x,t)');
title('Numerical solution');

figure;
surf(X, T, utrue);
shading faceted;
xlabel('x');
ylabel('Time');
zlabel('S(x,t)');
title('True solution');

figure;
surf(X, T, utrue - u');
colormap winter;
xlabel('x');
ylabel('t');
zlabel('Error');
title('Error');

%%
figure;
surf(X, T, v');
shading interp;
xlabel('x');
```

```
ylabel('Time');
zlabel('R(x,t)');
title('Numerical solution');

figure;
surf(X, T, vtrue);
shading faceted;
xlabel('x');
ylabel('Time');
zlabel('R(x,t)');
title('True solution');

figure;
surf(X, T, vtrue - v');
colormap winter;
xlabel('x');
ylabel('t');
zlabel('Error');
title('Error');

%%
figure;
surf(X, T, w');
shading interp;
xlabel('x');
ylabel('Time');
zlabel('T(x,t)');
title('Numerical solution');

figure;
surf(X, T, wtrue);
shading faceted;
xlabel('x');
ylabel('Time');
zlabel('T(x,t)');
title('True solution');

figure;
surf(X, T, wtrue - w');
colormap winter;
xlabel('x');
ylabel('t');
zlabel('Error');
title('Error');

function [u1,v1,w1] = initial(x)
global rho k1 k2
u1 = rho/10*x;
v1 = 4*rho/10*x;
w1 = 5*rho/10*x;
end
```

```
function [u,v,w] = truesol(x,t)
global rho k1 k2
u = 2*rho*x./(k1*k2*t.^2 + 2*(k1 + 4*k2)*t + 20);
v = 2*rho*x.*(k1*t + 4)./(k1*k2*t.^2 + 2*(k1 + 4*k2)*t + 20);
w = rho*x.*(k1*k2*t.^2 + 8*k2*t + 10)./(k1*k2*t.^2 + 2*(k1 + 4*k2)*t + 20);
end

function [x,t,u,v,w] = MOC(x0,xend,t0,tend,Nx,Nt)
global rho k1 k2
x = linspace(x0,xend,Nx); % Space grid
t = linspace(t0,tend,Nt); % Time grid
dx = (xend - x0)/(Nx - 1);
dt = (tend - t0)/(Nt - 1);

% Numerical solution
[u1,v1,w1] = initial(x);
u = zeros(Nx,Nt);
v = zeros(Nx,Nt);
w = zeros(Nx,Nt);
% Initial value
u(:,1) = u1;
v(:,1) = v1;
w(:,1) = w1;

% Method of characteristic
for n = 1:Nt - 1

    % Interpolate value from previous time step
    unew = u(:,n);
    vnew = v(:,n) + dt*k1*u(:,n);
    wnew = w(:,n) + dt*k2*v(:,n);

    % Compute characteristics
    x_char = x + dt/rho*(k1*transpose(u(:,n)) + k2*transpose(v(:,n)));

    % Update numerical solution
    u(:,n + 1) = interp1(x_char, unew, x, 'spline', 'extrap');
    v(:,n + 1) = interp1(x_char, vnew, x, 'spline', 'extrap');
    w(:,n + 1) = interp1(x_char, wnew, x, 'spline', 'extrap');
end
end
```

References

[1] Céline Hervieu, Niki Christou, Serge Battu, and Muriel Mathonnet. The role of cancer stem cells in colorectal cancer: from the basics to novel clinical trials. *Cancers*, 13(5):1092, 2021.

[2] Bruce M Boman, Rhonda Walters, Jeremy Z Fields, Albert J Kovatich, Tao Zhang, Gerald A Isenberg, Scott D Goldstein, and Juan P Palazzo. Colonic crypt changes during adenoma development in familial adenomatous polyposis: immunohistochemical evidence for expansion of the crypt base cell population. *The American journal of pathology*, 165(5):1489–1498, 2004.

[3] Geovan CM Campos, José Augusto Ferreira, and Giuseppe Romanazzi. Density-pressure ibvp: Numerical analysis, simulation and cell dynamics in a colonic crypt. *Applied Mathematics and Computation*, 424:127037, 2022.

[4] Kieran Smallbone and Bernard M Corfe. A mathematical model of the colon crypt capturing compositional dynamic interactions between cell types. *International journal of experimental pathology*, 95(1):1–7, 2014.

[5] IP Tomlinson and WF Bodmer. Failure of programmed cell death and differentiation as causes of tumors: some simple mathematical models. *Proceedings of the National Academy of Sciences*, 92(24):11130–11134, 1995.

[6] Matthew D Johnston, Carina M Edwards, Walter F Bodmer, Philip K Maini, and S Jonathan Chapman. Mathematical modeling of cell population dynamics in the colonic crypt and in colorectal cancer. *Proceedings of the National Academy of Sciences*, 104(10):4008–4013, 2007.

[7] Frank A Meineke, Christopher S Potten, and Markus Loeffler. Cell migration and organization in the intestinal crypt using a lattice-free model. *Cell proliferation*, 34(4):253–266, 2001.

[8] Bruce M Boman, Arthur Guetter, Ryan M Boman, and Olaf A Runquist. Autocatalytic tissue polymerization reaction mechanism in colorectal cancer development and growth. *Cancers*, 12(2):460, 2020.

[9] Kapil Chawla Maruf Lawal Soheil Saghafi Sandra Annie Tsiorintsoa Chahat Upreti Khoi Vo Amanda Albright, Maia Van Bonn. Symmetric and asymmetric cell division and modeling of interacting cell populations in the colonic crypt.

[10] Konstantinos Mamis, Ruibo Zhang, and Ivana Bozic. Stochastic model for cell population dynamics quantifies homeostasis in colonic crypts and its disruption in early tumorigenesis. *Proceedings of the Royal Society B*, 290(2009):20231020, 2023.

[11] Elham Raeisi, Mehmet Yavuz, Mohammadreza Khosravifarsani, and Yasin Fadaei. Mathematical modeling of interactions between colon cancer and immune system with a deep learning algorithm. *The European Physical Journal Plus*, 139(4):345, 2024.

[12] Eric J Puttock. *Patterned Heterogeneity in Colon Cancer: Data-driven, Mechanistic Mathematical Modeling*. University of California, Irvine, 2020.